Brittle fracture in a periodic structure with internal potential energy. Spontaneous crack propagation

Ayzenberg-Stepanenko, Mark; Mishuris, Gennady; Slepyan, Leonid

Published in:
Proceedings of the Royal Society A: Mathematical, Physical and Engineering Sciences

DOI:
10.1098/rspa.2014.0121

Publication date:
2014

Citation for published version (APA):
Ayzenberg-Stepanenko, M., Mishuris, G., & Slepyan, L. (2014). Brittle fracture in a periodic structure with internal potential energy. Spontaneous crack propagation. *Proceedings of the Royal Society A: Mathematical, Physical and Engineering Sciences*, *470*(2167), [20140121]. https://doi.org/10.1098/rspa.2014.0121

PROCEEDINGS OF THE ROYAL SOCIETY A

rspa.royalsocietypublishing.org

Brittle fracture in a periodic structure with internal potential energy. Spontaneous crack propagation

Mark Ayzenberg-Stepanenko[1], Gennady Mishuris[2] and Leonid Slepyan[2,3]

[1]The Shamoon College of Engineering, Beer-Sheva 84105, Israel
[2]Institute of Mathematics and Physics, Aberystwyth University, Ceredigion, Wales SY23 3BZ, UK
[3]School of Mechanical Engineering, Tel Aviv University, PO Box 39040, Ramat Aviv, 69978 Tel Aviv, Israel

Research

Cite this article: Ayzenberg-Stepanenko M, Mishuris G, Slepyan L. 2014 Brittle fracture in a periodic structure with internal potential energy. Spontaneous crack propagation. *Proc. R. Soc. A* **470**: 20140121.
http://dx.doi.org/10.1098/rspa.2014.0121

Received: 12 February 2014
Accepted: 4 April 2014

Subject Areas:
applied mathematics, mechanics, materials science

Keywords:
periodic structure, failure waves, dynamic fracture

Author for correspondence:
Leonid Slepyan
e-mail: slepyanl@post.tau.ac.il

Spontaneous brittle fracture is studied based on the model of a body, recently introduced by two of the authors, where only the prospective crack path is specified as a discrete set of alternating initially stretched and compressed bonds. In such a structure, a bridged crack destroying initially stretched bonds may propagate under a certain level of the internal energy without external sources. The general analytical solution with the crack speed–energy relation is presented in terms of the crack-related dynamic Green's function. For anisotropic chains and lattices considered earlier in quasi-statics, the dynamic problems are examined and discussed in detail. The crack speed is found to grow unboundedly as the energy approaches its upper limit. The steady-state sub- and supersonic regimes found analytically are confirmed by numerical simulations. In addition, irregular growth, clustering and crack speed oscillation modes are detected at a lower bound of the internal energy. It is observed, in numerical simulations, that the spontaneous fracture can occur in the form of a pure bridged, partially bridged or fully open crack depending on the internal energy level.

1. Introduction

We consider a spontaneous crack propagating in a structural elastic body with periodically distributed, self-equilibrated, microlevel stresses. No external forces

Royal Society Publishing

are assumed to be applied. The analysis is based on the model introduced in [1], where the static states were examined. In the general formulation, an unspecified periodic structure is considered, where only the prospective crack path is specified as a discrete set of alternating stretched and compressed bonds. In particular, such an incompatible stress distribution may occur if the bonds are of different initial lengths (figure 1*a*). The general analytical solution corresponds to the bridged crack propagating with a constant speed and destroying the initially stretched bonds. The solution is obtained in terms of the crack-related dynamic Green's function for an unspecified periodic structure. The selective discrete Fourier transform introduced in [1] is used in a dynamical setting.

The solution represents the internal energy level as a uniquely defined function of the crack speed. The inverse, multi-valued function usually is uniquely defined by the admissibility condition [2], which states, in general, that a bond should not rise above the breaking point before the moment assumed in the problem formulation. It follows that only the maximal speed corresponding to the given energy is realized. However, if two or more close minima of the energy exist corresponding to different values of the speed, then the latter can oscillate. The revealed phenomenon of instability manifests itself in the case of a two-line chain considered below. In this connection, note that there are some (numerical) examples where cracks have two bistable regimes for the same energy release [3].

Along with the general structure, two specified structures, the mass-spring lattice and two-line chain, are considered in detail. For these structures, quantitative results are obtained based on the general solution and the specific Green's functions. We also present results of the numerical simulations of the corresponding transient problems. This allows us to determine the regions of stability of the analytical solutions and to reveal unsteady regimes as well as partially bridged and fully open crack propagation modes. For the structures under consideration, the analytical results are specified for an arbitrary value of the parameter defining the structure's anisotropy. Note that the anisotropy plays a substantial role in this problem.

There are two bounds of the internal energy, and the spontaneous crack can exist in the energy segment between them. It cannot propagate if the energy is below the lower bound, whereas the intact structure cannot exist if the energy exceeds the upper bound. The corresponding speed–energy relations are obtained analytically and plotted for the specified structures. The speed range extends from a non-zero value and, in the considered model, has no upper bound. The speed tends to infinity as the energy level approaches its upper bound. The numerical simulations show that, at a high level of the internal energy, not only the stretched bonds, but also the initially compressed ones will break. So, the spontaneous failure wave can propagate in the form of a pure bridged, partially bridged or fully open crack depending on the internal energy level.

Note that, in some respects, the problem is related to that for the bridge crack [4,5], to the weak-bond fracture of a lattice [6] and to the transition waves in bistable structures [7–10]. In a sense, the spontaneous crack propagation considered below also relates to the so-called Prince Rupert's drop phenomenon of disintegration, first noted in the seventeenth century [**?**] and to the fragmentation of metastable glass [12]. These phenomena can be referred to the internal potential energy, which releases under a local breakage, resulting in the spontaneous disintegration.

The state of the considered structure is characterized by the following values. The first is the *initial internal energy*, $\mathcal{E}$, which arises owing to the difference in the interface bond lengths and stored in the cell of periodicity, that is, in two spans of the structure. Next is the *initial energy of the bond*, E, which is the same for all the bonds. These two values correspond to the initial state of the intact structure. Finally, there is the *actual energy of the bond*, E_m, where m is the bond number. These energies refer to the microlevel scale.

The critical values of the initial internal energy and the bond energy are denoted by $\mathcal{E}_c$ and E_c, respectively. The latter is the same for all of the bonds; it relates to the critical extension. Note that $E = E_c$ under $\mathcal{E} = \mathcal{E}_c$. The level of the internal energy is characterized by the *ratio of the stored internal energy to its critical value*, $\gamma = \mathcal{E}/\mathcal{E}_c = E/E_c$.

In the formulation, the displacements about the initial positions of unstrained bond ends are introduced in terms of the initial and actual states, $\mathcal{U}_m$ and $u_m = \mathcal{U}_m + U_m(t)$, respectively,

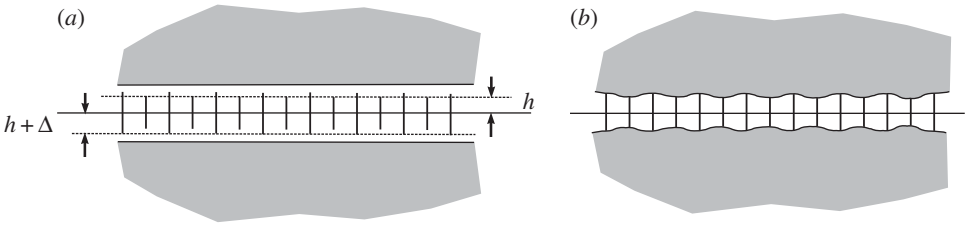

Figure 1. (*a*,*b*) The body with the structured interface. The compressed and stretched bonds alternate creating self-equilibrated stresses.

where m is the bond number. It is assumed that the bond stiffnesses are the same. In this case, in the initial state

$$\mathcal{U}_{2m} = -\mathcal{U}_{2m+1} = \text{const}, \quad m = 0, \pm 1, \ldots. \tag{1.1}$$

In the analytical study, we consider the bridged crack as the breakage of initially stretched bonds propagating in the *steady-state* mode. We use this term assuming that the dynamic state is characterized by two functions of one argument, $\eta = t - \tau m$, but not on t and m separately (a constant crack speed $v = 1/\tau$). Numerical simulations demonstrate that the steady-state solutions found analytically really exist. In addition, the simulations reveal more complicated ordered modes with crack speed oscillations, where periodic clusters consist of two or more initially stretched bonds.

For the specified structures, we determine the lower values of $\gamma = \gamma_c$ as a function of an orthotropy parameter, α, as the lower bound of the domain where the bridge crack may propagate spontaneously. As a manifestation of the dynamic amplification factor (see [13]), this bound appears considerably below its static values found in [1]. Next, we determine the crack speed as a function of γ, $\gamma_c \le \gamma < 1$. In the numerical simulations, it appears that the steady-state regime is quickly established if parameter γ is not too close to γ_c. Otherwise, the crack speed is unstable and can be very low. It becomes supersonic and grows unboundedly for $\gamma \to 1$. Moreover, in this case, not only can initially stretched bonds break as assumed in the analytical formulation, but also the initially compressed bonds become broken, and an open propagating crack forms with a finite bridged region.

2. Analytical study of a general problem

(a) Problem formulation

We consider two equal half-planes or layers of a non-specified periodic structure connected by a set of elastic bonds (figure 1*b*). The bonds are numbered by $m = 0, \pm 1, \ldots$. The between-the-bond distance is taken as the length unit. The even and odd bonds differ only by their initial length, namely the even bonds, $m = 0, \pm 2, \ldots$, are of the length $2h$, whereas the odd bonds, $m = \pm 1, \pm 3, \ldots$, are of a slightly different length, $2h + 2\Delta$ with $\Delta > 0$, $\Delta/h \ll 1$. In the framework of Hooke's law, the bond's stiffness, $\varkappa$, is assumed to be the same for both the even and the odd bonds, and the response of the structure to external forces corresponds to the regular, periodic set of the bonds. This also concerns the bulk of the body, where the internal energy may be present.

If the internal energy level is sufficient, then a spontaneous breakage of the even bonds can propagate along the interface in the absence of external forces. We assume that the steady-state regime can exist, where the dynamic displacements of the upper knots of the interface, additional to those in the initial state, are described by two different functions of a single argument, one function for the even bonds and the other for the odd ones

$$U_m(t) = U(\eta) \ \ (m = 0, \pm 2, \ldots), \quad U_m(t) = V(\eta) \ \ (m = \pm 1, \pm 3, \ldots), \quad \eta = t - \tau m. \tag{2.1}$$

Note that, in this notation, the bridged crack speed is $v = 1/\tau$.

The structure's dynamic properties are reflected by the Green's function considered below. The initial displacements of the upper knots of the interface are defined by the static solution presented in [1]. The additional displacements satisfy the relations (2.1). No even bonds exist at $\eta > 0$ (it is the bridged crack area), whereas the structure is intact at $\eta \leq 0$. The conditions at infinity correspond to the absence of external actions.

In analytical calculations, the crack speed, v, is defined by the internal energy, $\mathcal{E}$. However, as is common in such mixed boundary value problems, we solve analytically the inverse problem considering v as an input parameter, which is far more convenient. Herewith, the graphs also plotted for the inverse problem solution allow us to see the direct dependence, $v(\mathcal{E})$.

Recall that the inverse, multi-valued function is usually uniquely defined by the admissibility condition. Namely the bond strain energy before the fracture point must be below the critical value. It follows from this that, among the speeds which are found to correspond to a given level of the internal energy, only the maximal speed is acceptable [2] and that the results for $\gamma(v) > 1$ are not acceptable. In addition, the results obtained under this formulation are valid if the odd-number bond dynamic states remain subcritical. Note that the numerical simulations discussed in §5 confirm the analytical results for the whole range of γ. Interestingly, in the case where γ is close to one, the odd bonds also become broken, but this does not influence the crack speed.

Mathematically, we consider the intact structure under self-equilibrated external forces, $Q(\eta)$, acting in the opposite directions on the upper and lower ends of the even bonds. These forces, which are unknown in advance, serve to compensate the tensile forces in the even bonds at $\eta > 0$

$$Q(\eta) = Q_0(\eta) = 2\varkappa u_0(\eta) = 2\varkappa[\mathcal{U}_0 + U(\eta)] \quad (m = 0, \pm 2, \ldots), \tag{2.2}$$

where $\varkappa$ is the bond stiffness. The task is to determine the dynamic displacements, whereas the initial displacements found in [1] are

$$\mathcal{U}_0 = -\mathcal{U}_1 = \Delta L(0), \tag{2.3}$$

where $L(k)$ is the kernel of the static version of the Wiener–Hopf equation. Note that $L(0)$ takes the same value in both the dynamic and static formulations.

(b) Dynamic Green's functions

In the analysis, we consider the dynamic crack-related Green's function, $G(m, t)$, corresponding to the intact structure under unit self-equilibrated pulses acting at $t = 0$ in opposite directions on the upper and lower ends of the bond $m = 0$. It then follows that the dynamic displacements, $U(\eta)$ and $V(\eta)$, are

$$\left.\begin{aligned} U(\eta) &= \sum_{m'=0,\pm 2,\ldots} G(m - m', t) * Q_0(t - \tau m') \quad (m = 0, \pm 2, \ldots) \\ \text{and} \qquad V(\eta) &= \sum_{m'=0,\pm 2,\ldots} G(m - m', t) * Q_0(t - \tau m') \quad (m = \pm 1, \pm 3, \ldots), \end{aligned}\right\} \tag{2.4}$$

where the asterisk means the convolution on t.

Below the Fourier transform on t and the discrete Fourier transform on m are denoted by the superscript F, whereas the continuous Fourier transform on η is denoted by the superscript F_η. The latter leads to the following relations

$$\left.\begin{aligned} U^{F_\eta}(k) &= \int_{-\infty}^{\infty} U(\eta)\, \mathrm{e}^{\mathrm{i}k\eta}\, \mathrm{d}\eta = Q_0^{F_\eta}(k) \sum_{m'=0,\pm 2,\ldots} G^F(m - m', k)\, \mathrm{e}^{-\mathrm{i}k\tau(m-m')} \\ \text{and} \qquad V^{F_\eta}(k) &= \int_{-\infty}^{\infty} V(\eta)\, \mathrm{e}^{\mathrm{i}k\eta}\, \mathrm{d}\eta = Q_0^{F_\eta}(k) \sum_{m'=0,\pm 2,\ldots} G^F(m - m', k)\, \mathrm{e}^{-\mathrm{i}k\tau(m-m')} \end{aligned}\right\} \tag{2.5}$$

with

$$Q_0^{F_\eta}(k) = \int_0^{\infty} Q_0(t)\, \mathrm{e}^{\mathrm{i}k\eta}\, \mathrm{d}\eta. \tag{2.6}$$

Thus,

$$U^{F_\eta}(k) = Q_0^{F_\eta}(k)\mathcal{G}_{\text{even}}(k), \quad V^{F_\eta}(k) = Q_0^{F_\eta}(k)\mathcal{G}_{\text{odd}}(k). \tag{2.7}$$

The functions $\mathcal{G}_{\text{even}}(k)$ and $\mathcal{G}_{\text{odd}}(k)$ are the double Fourier transforms, the continuous transform on t with the parameter k and the selective discrete transforms on m (on even m and on odd m separately) with the parameter $-\tau k$

$$\left.\begin{aligned} \mathcal{G}_{\text{even}}(k) &= G^{FF}_{\text{even}}(-\tau k, k) = \sum_{m=0,\pm2,\dots} \int_{-\infty}^{\infty} G(m,t)\, \mathrm{e}^{\mathrm{i}kt - \mathrm{i}\tau km}\, \mathrm{d}t \\ \text{and} \qquad \mathcal{G}_{\text{odd}}(k) &= G^{FF}_{\text{odd}}(-\tau k, k) = \sum_{m=\pm1,\pm3,\dots} \int_{-\infty}^{\infty} G(m,t)\, \mathrm{e}^{\mathrm{i}kt - \mathrm{i}\tau km}\, \mathrm{d}t. \end{aligned}\right\} \tag{2.8}$$

The selective transforms introduced in [1] can be expressed in terms of the regular discrete transform as follows:

$$\left.\begin{aligned} \mathcal{G}_{\text{even}}(k) &= G^{FF}_{\text{even}}(-\tau k, k) = \tfrac{1}{2}\left[G^{FF}(-\tau k, k) + G^{FF}(-\tau k + \pi, k)\right] \\ \text{and} \qquad \mathcal{G}_{\text{odd}}(k) &= G^{FF}_{\text{odd}}(-\tau k, k) = \tfrac{1}{2}\left[G^{FF}(-\tau k, k) - G^{FF}(-\tau k + \pi, k)\right], \end{aligned}\right\} \tag{2.9}$$

with

$$G^{FF}(-\tau k, k) = \sum_{m=0,\pm1,\dots} \int_{-\infty}^{\infty} G(m,t)\, \mathrm{e}^{\mathrm{i}kt - \mathrm{i}\tau km}\, \mathrm{d}t. \tag{2.10}$$

(c) The spontaneous bridge crack propagation

Let the breakage of the even bonds propagate with constant speed, $v = 1/\tau > 0$, and let the damaged area be for $\eta = t - m\tau > 0$, whereas the intact bond area is for $\eta \le 0$. We can consider this structure as completely intact, but under the external forces, $Q_0(\eta)$, which compensate for the actions of the even bonds at $\eta > 0$. These forces are defined in (2.2). The Fourier transform leads to

$$\left.\begin{aligned} Q_0^{F_\eta}(k) &= 2\varkappa u_+(k) = 2\varkappa\left(U_+(k) + \frac{\mathcal{U}_0}{(0 - \mathrm{i}k)}\right) \\ \text{and} \qquad U^{F_\eta}(k) &= U_+(k) + U_-(k), \quad U_\pm(k) = \int_{-\infty}^{\infty} U(\eta)\, \mathrm{e}^{\mathrm{i}k\eta} H(\pm\eta)\, \mathrm{d}\eta. \end{aligned}\right\} \tag{2.11}$$

Recall that $\mathcal{U}_0 = -\mathcal{U}_1$ are the initial displacements (2.3) caused by the microlevel stresses.

Now the governing equations follow from (2.7) as

$$\left.\begin{aligned} U^{F_\eta}(k) &= 2\varkappa\mathcal{G}_{\text{even}}(k)\left(U_+(k) + \frac{\mathcal{U}_0}{(0 - \mathrm{i}k)}\right) \\ \text{and} \qquad V^{F_\eta}(k) &= 2\varkappa\mathcal{G}_{\text{odd}}(k)\left(U_+(k) + \frac{\mathcal{U}_0}{(0 - \mathrm{i}k)}\right). \end{aligned}\right\} \tag{2.12}$$

The first of the equations in (2.12) is independent of the second. It is the Wiener–Hopf-type equation with respect to the dynamic displacements of the even bonds

$$U_-(k) + L(k)U_+(k) = [1 - L(k)]\,\frac{\mathcal{U}_0}{(0 - \mathrm{i}k)}, \quad L(k) = 1 - 2\varkappa\mathcal{G}^F_{\text{even}}(k), \tag{2.13}$$

where $\mathcal{G}_{\text{even}}(k)$ is expressed through the original Green's function $G^{FF}(-\tau k, k)$ in (2.9).

We assume that the function $L(k)$ satisfies the conditions which allow us to solve this equation in a regular way (in this connection, see [8, pp. 449–451]). To proceed, the factorization

should be made as

$$L(k)=\lim_{\Im k\to 0} L_+(k)L_-(k),\quad L_\pm(k)=\exp\left[\pm\frac{1}{2\pi \mathrm{i}}\int_{-\infty}^{\infty}\frac{\ln L(\xi)}{\xi-k}\,\mathrm{d}\xi\right]\quad(\pm\Im k>0). \tag{2.14}$$

In particular, it follows from this that

$$L_\pm(\pm \mathrm{i}\infty)=1,\quad L_\pm(0)=\sqrt{L(0)}\,\mathcal{R}^{\pm 1},\quad \mathcal{R}=\exp\left[\frac{1}{\pi}\int_0^{\infty}\frac{\mathrm{Arg}L(\xi)}{\xi}\,\mathrm{d}\xi\right]. \tag{2.15}$$

Next, we represent equation (2.13) in a form where the plus/minus functions are separated

$$\left.\begin{aligned}&\frac{U_-(k)}{L_-(k)}+L_+(k)U_+(k)=\frac{\mathcal{U}_0}{0-\mathrm{i}k}\left[\frac{1}{L_-(k)}-L_+(k)\right]=C_+(k)+C_-(k)\\ \text{and}\qquad &C_+(k)=\frac{\mathcal{U}_0}{0-\mathrm{i}k}\left[\frac{1}{L_-(0)}-L_+(k)\right],\quad C_-(k)=\frac{\mathcal{U}_0}{0-\mathrm{i}k}\left[\frac{1}{L_-(k)}-\frac{1}{L_-(0)}\right].\end{aligned}\right\} \tag{2.16}$$

In the considered case, it follows that

$$U_+(k)=\frac{\mathcal{U}_0}{0-\mathrm{i}k}\left[\frac{1}{L_-(0)L_+(k)}-1\right],\quad U_-(k)=\frac{\mathcal{U}_0}{0-\mathrm{i}k}\left[1-\frac{L_-(k)}{L_-(0)}\right] \tag{2.17}$$

and

$$\left.\begin{aligned}&U(0)=\lim_{k\to-\mathrm{i}\infty}\mathrm{i}kU_-(k)=\lim_{k\to\mathrm{i}\infty}(-\mathrm{i}k)U_+(k)=\mathcal{U}_0\left(\frac{1}{L_-(0)}-1\right)\\ \text{and}\qquad &u_0(0)=\frac{\mathcal{U}_0}{L_-(0)}=\frac{\mathcal{U}_0\mathcal{R}}{\sqrt{L(0)}}.\end{aligned}\right\} \tag{2.18}$$

To calculate this value for a specific structure the integral transform of the original Green's function, $G^{FF}(-\tau k,k)$, should be specified. As for $V(\eta)$, its transform, $V^F(k)$, is defined by the last relation in (2.12), where $U_+(k)$ is now known (2.17).

(d) Energy relations

The critical strain energy, E_c, is crack-speed independent

$$E_\mathrm{c}=2\varkappa u_\mathrm{c}^2, \tag{2.19}$$

where u_c is the critical displacement. The internal energy density per two span, $\mathcal{E}$, is (see [1])

$$\mathcal{E}=2\varkappa\Delta^2 L(0). \tag{2.20}$$

We introduce the ratio

$$\gamma=\frac{\mathcal{E}}{\mathcal{E}_\mathrm{c}}=\frac{\mathcal{U}_0^2}{u_\mathrm{c}^2}, \tag{2.21}$$

where $\mathcal{E}_\mathrm{c}$ is the critical internal energy: $\mathcal{E}=\mathcal{E}_\mathrm{c}$ as $E=E_\mathrm{c}$ in the initial state. At the moment of the bond breakage, the total displacement $\mathcal{U}_0+U(0)=u_\mathrm{c}$, and it follows from (2.18) that

$$\gamma=L_-^2(0)=L(0)\mathcal{R}^{-2}. \tag{2.22}$$

Note that the right-hand side of (2.22) is a function of the crack speed. So this relation serves for the determination of the crack speed as a function of γ. Recall that (2.22) may be satisfied by a number of values of v. Usually [2], only the maximal value of the speed is considered to be admissible, because it corresponds to the first moment when the bond state becomes critical. There are some exceptions, however, as we show below.

The fracture energy itself is found based on (2.18), (2.20) and (2.3). It is

$$E_\mathrm{f}=2\varkappa(\mathcal{U}_0+U(0))^2=2\varkappa\mathcal{U}_0^2L_-^{-2}(0)\mathcal{R}^2=2\varkappa\Delta^2L(0)\mathcal{R}^2. \tag{2.23}$$

Thus, the ratio of the fracture energy to the internal energy, $\mathcal{E}$, is

$$R_\mathrm{f}=\frac{E_\mathrm{f}}{\mathcal{E}}=\mathcal{R}^2=\exp\left[\frac{2}{\pi}\int_0^{\infty}\frac{\mathrm{Arg}L(\xi)}{\xi}\,\mathrm{d}\xi\right]=\frac{L(0)}{\gamma}. \tag{2.24}$$

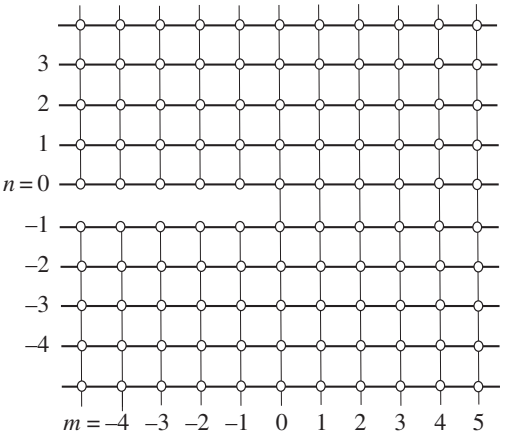

Figure 2. The orthotropic lattice. The stiffness of the horizontal and vertical bonds is μ and $\varkappa$, respectively ($\alpha = \varkappa/\mu$). The bonds on the crack line are prestressed as defined earlier.

3. Two specific structures

Here, we consider the same specific structures as in [1]: the two-line chain and the orthotropic square lattice, but we take into account point masses placed at the knots (figure 2). The spontaneous failure waves in these structures demonstrate a non-trivial dependence on the internal energy level and the anisotropy parameter. Below, we illustrate and discuss this in detail.

(a) The two-line chain

The dynamics of the chain shown in figure 3 is governed by the equation

$$M\ddot{u}_m(t) + 2(\varkappa + \mu)u_m(t) - \mu(u_{m+1}(t) + u_{m-1}(t)) = \pm Q(m,t), \tag{3.1}$$

where signs $\pm$ correspond for the upper and lower line, respectively. From this, the Green's function $G(m,t)$ is defined as the displacements corresponding to $Q(m,t) = \delta(t)\delta_{m,0}$. We find

$$G^{FF}(-\tau k, k) = \left(\frac{1}{\mu}\right)\left[\left(0 - \frac{\mathrm{i}k}{c}\right)^2 + 2(\alpha + 1 - \cos\tau k)\right]^{-1}, \quad c = \sqrt{\frac{\mu}{M}}. \tag{3.2}$$

It follows that

$$\left.\begin{aligned}
&\mathcal{G}_{\mathrm{even}} = \frac{1}{\mu}\frac{(0 - \mathrm{i}k/c)^2 + 2(\alpha+1)}{[(0 - \mathrm{i}k/c)^2 + 2(\alpha+1)]^2 - 4\cos^2\tau k},\\
&\mathcal{G}_{\mathrm{odd}} = \frac{1}{\mu}\frac{2\cos\tau k}{[(0 - \mathrm{i}k/c)^2 + 2(\alpha+1)]^2 - 4\cos^2\tau k},\\
&L_1(k) = \left(0 - \frac{\mathrm{i}k}{c}\right)^4 + 2(\alpha+2)\left(0 - \frac{\mathrm{i}k}{c}\right)^2 + 4\alpha + 4\sin^2\tau k,\\
&L_2(k) = \left(0 - \frac{\mathrm{i}k}{c}\right)^4 + 4(\alpha+1)\left(0 - \frac{\mathrm{i}k}{c}\right)^2 + 4\alpha(2+\alpha) + 4\sin^2\tau k\\
\text{and}\quad &L(k) = \frac{L_1(k)}{L_2(k)}, \quad L(0) = 1(2+\alpha).
\end{aligned}\right\} \tag{3.3}$$

Note that the dimension of $\tau, 1/k, 1/c$ is time. Along with this, because the distance between the bonds is taken as the length unit, c is the long wave speed. It can be seen below that the spontaneous failure wave can propagate with hypersonic speeds, $v = 1/\tau \gg c$.

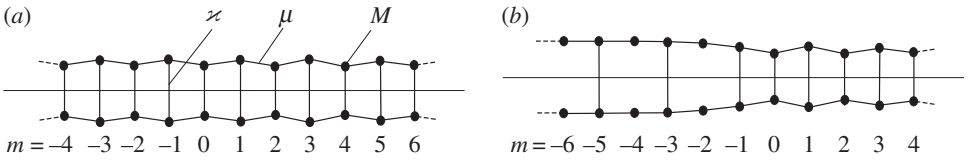

Figure 3. (*a*) The intact chain and (*b*) the chain with a semi-infinite bridged crack.

(i) Some limiting relations

We now derive some limiting relations that give us reference points for the dependencies presented below. Let us represent expressions corresponding to zero points of $L_{1,2}(k)$ in the form

$$\left.\begin{aligned} &\frac{k_{1,2}^2}{c^2} = \alpha + 2 \mp \sqrt{\alpha^2 + 4\cos^2 \tau k_{1,2}} \quad (L_1(k_{1,2}) = 0) \\ \text{and} \quad &\frac{k_{3,4}^2}{c^2} = 2(\alpha + 1) \mp 2|\cos \tau k_{3,4}| \quad (L_2(k_{3,4}) = 0). \end{aligned}\right\} \tag{3.4}$$

Note that these points correspond to waves radiated during the bridge crack propagation. Namely the numbers, k_i, $i = 1, \ldots, 4$, are the wave frequencies and τk_i are the wavenumbers.

Based on (3.3) and (3.4), we can find limiting relations corresponding to $\alpha = 0$, $\alpha = \infty$ and $v = 1/\tau = \infty$. In the case, $\alpha = 0$

$$L_1(k) = L_2(k), \quad \mathrm{Arg}L(k) = 0, \quad \mathcal{R} = 1, \quad L(0) = \tfrac{1}{2}, \tag{3.5}$$

and it follows from (2.22) that γ takes the static value, $\gamma = \frac{1}{2}$.

The same conclusion is valid for the opposite case, $\alpha \to \infty$, and also for $v \to \infty$ ($\tau \to 0$). We have

$$\left.\begin{aligned} &\frac{k_{1,2}}{c} = \sqrt{\alpha + 2 \mp \alpha} + o(1), \quad \frac{k_{3,4}}{c} = \sqrt{2\alpha} \mp \varepsilon_{1,2}, \quad \varepsilon_{1,2} = o(1) \ (\alpha \to \infty) \\ \text{and} \quad &\frac{k_{1,2}}{c} = \sqrt{\alpha + 2 \mp \sqrt{\alpha^2 + 4}}, \quad \frac{k_{3,4}}{c} = \sqrt{2(\alpha + 1) \mp 2} \ (v = \infty). \end{aligned}\right\} \tag{3.6}$$

In the considered cases, $\mathrm{Arg}L(k)$ is a piecewise constant function

$$\mathrm{Arg}L(k) = -\pi[H(k - k_1) + H(k - k_2) - H(k - k_3) - H(k - k_4)], \tag{3.7}$$

and

$$\mathcal{R} = \frac{k_1 k_2}{(k_3 k_4)}. \tag{3.8}$$

It follows that for any v

$$\mathcal{R} \sim \frac{1}{\sqrt{\alpha}}, \quad \gamma \sim \frac{1}{(\alpha \mathcal{R}^2)} \to 1 \ (\alpha \to \infty) \tag{3.9}$$

and for any α

$$\mathcal{R} = \frac{1}{\sqrt{\alpha + 2}}, \quad \gamma = \frac{1}{((\alpha + 2)\mathcal{R}^2)} = 1 \ (v = \infty). \tag{3.10}$$

Graphical illustrations of analytical results obtained for the chain are presented in §4 together with the results of numerical simulations.

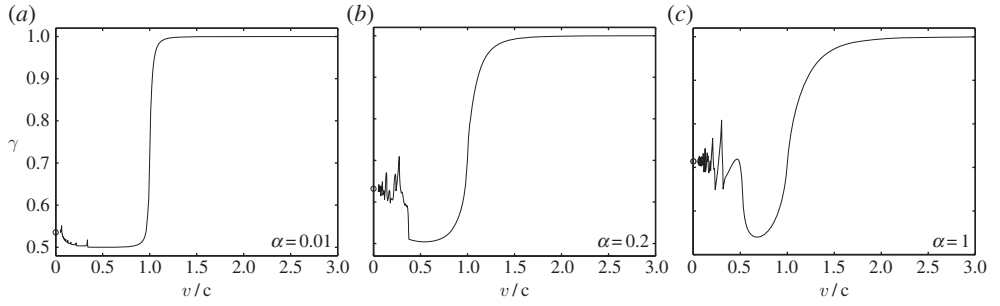

Figure 4. (*a–c*) The spontaneous bridge crack in the lattice. The evolution of the $\gamma - v/c$ dependence when changing the anisotropy parameter α. Recall that $\gamma = \mathcal{E}/\mathcal{E}_c$ is the ratio of the internal energy to its critical value. The blurred minimum, where an unsteady crack speed regime can be expected, and a jump-like dependence corresponding to small α. The minimum becomes more localized as α grows.

(b) The square-cell lattice

From the equation for the lattice dynamics under unit self-equilibrated pulses

$$M\ddot{u}_{m,n}(t) + 2(\varkappa + \mu)u_{m,n}(t) - \mu(u_{m+1,n}(t) + u_{m-1,n}(t)) - \varkappa(u_{m,n+1}(t) + u_{m,n-1}(t)) = \delta(t)\delta_{m,0}[\delta_{n,0} - \delta_{n,-1}] \tag{3.11}$$

we find the double Fourier transform of the crack-related dynamic Green's function

$$\left.\begin{aligned} G^{FF}(-\tau k, k) &= \frac{1}{2\varkappa}\left(1 - \sqrt{\frac{Y + 4\sin^2 \tau k/2}{Y + 4\sin^2 \tau k/2 + 4\alpha}}\right), \\ L(k) &= \frac{1}{2}\left(\sqrt{\frac{Y + 4\sin^2 \tau k/2}{Y + 4\sin^2 \tau k/2 + 4\alpha}} + \sqrt{\frac{Y + 4\cos^2 \tau k/2}{Y + 4\cos^2 \tau k/2 + 4\alpha}}\right) \\ \text{and} \quad L(0) &= \frac{1}{(2\sqrt{\alpha + 1})}, \quad Y = \left(0 - \frac{\mathrm{i}k}{c}\right)^2, \quad c = \sqrt{\frac{\mu}{M}}. \end{aligned}\right\} \tag{3.12}$$

Note that such a lattice in the absence of the internal energy was considered in [14] without evaluation of the Green's function (also see [15]).

The limiting relations following from (2.22) and (3.12) are

$$\gamma\left(\frac{v}{c}, \alpha\right) \to \frac{1}{2} \ (\alpha \to 0), \quad \gamma\left(\frac{v}{c}, \alpha\right) \to \gamma_\infty\left(\frac{v}{c}\right) = \frac{1}{2}\exp\left[-\frac{2}{\pi}\int_0^2 \frac{\mathrm{Arg}L^*(k)}{k}\,\mathrm{d}k\right] \ (\alpha \to \infty), \tag{3.13}$$

where

$$L^*(k) = \sqrt{(0 - \mathrm{i}k)^2 + 2(1 - \cos \tau ck)} + \sqrt{(0 - \mathrm{i}k)^2 + 2(1 + \cos \tau ck)}. \tag{3.14}$$

It is found from this that in the limit, $\alpha \to \infty$, the minimal value of γ and the corresponding speed are $\gamma \approx 0.66656$, $v/c \approx 0.709$ (figure 6*a*, where $\gamma_{\min}(\alpha)$ is plotted).

(i) Graphical illustrations of the analytical results for the lattice

Here, we present the energy–speed relation plotted for some values of α in figures 4 and 5 in the form of the dependence of the normalized internal energy, $\gamma = \mathcal{E}/\mathcal{E}_c$, on the normalized crack speed, v/c.

It can be seen that the minimal admissible speed is about a half of the long wave speed, c. So, there is no slow crack in this case. This is the same as for the open crack in the isotropic lattice under remote forces [16,17]. However, in contrast to the latter case, the crack in the lattice with

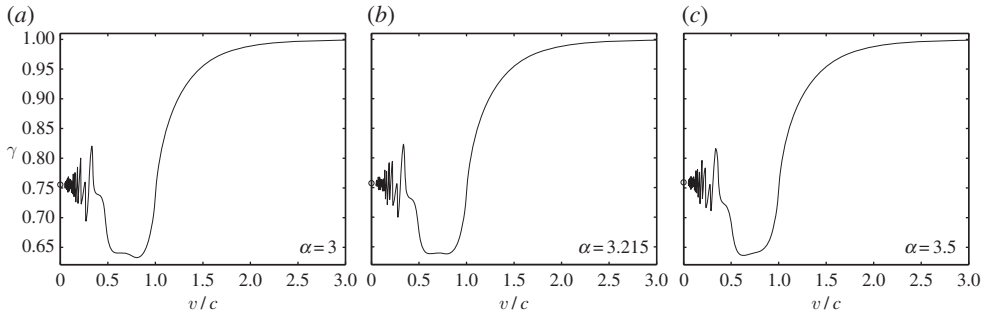

Figure 5. (*a–c*) The spontaneous bridge crack in the lattice. The evolution of the $\gamma - v/c$ dependence with the anisotropy parameter α. In these plots, one can see how the minimum bifurcates and changes location with a relatively small change of the anisotropy parameter α. The presence of two concurrent minima ($\alpha = 3.215$) may lead to crack speed oscillations about a stable averaged value.

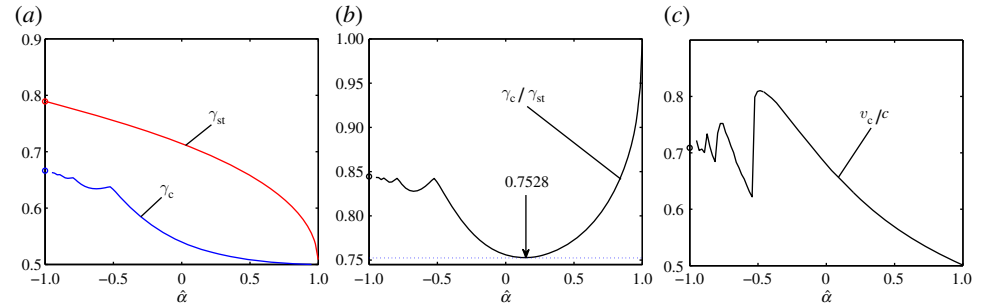

Figure 6. The spontaneous bridge crack in the lattice: the dynamic, γ_c, and static, γ_{st}, values of the minimal γ, which is sufficient for the spontaneous crack to exist, as a function of the normalized anisotropy parameter, $\hat{\alpha} = (1-\alpha)/(1+\alpha)$ (*a*,*b*), and the corresponding crack speed (*c*). The small circles correspond to the limiting values found in §3*b*. (Online version in colour.)

internal energy can propagate at any high speed, the long wave speed is no longer the crack speed limit. Indeed, the crack gets its energy from the source distributed over its path, not from any forces acting at a distance.

In figures 4 and 5, a non-trivial role of the anisotropy can be seen: the blurred minimum, where an unsteady crack speed regime can be expected, a jump-like dependence corresponding to small α and the localization of the minimum with growing α (figure 4). In the range $3 \leq \alpha \leq 3.5$, the minimum bifurcates and changes location, and we have two equal minima at $\alpha = 3.215$ (figure 5). Uncertainty of the crack speed arises in this case. As discussed in §4, such a configuration results in crack speed oscillations between these minima. This phenomenon resembles the clustering revealed earlier (see [5,18]).

The minimal γ as a function of the normalized anisotropy parameter, $\hat{\alpha} = (1-\alpha)/(1+\alpha)$, the dynamic and static values, and the corresponding crack speed are presented in figure 6. Note that the minimal values of the internal energy required for the spontaneous crack growth initiation (in the static formulation) and propagation (the dynamic formulation) differ greatly. The decrease of the latter in comparison with the former arises owing to the dynamic factor [13]. It is remarkable that there exists a jump in the dependence of the corresponding speed on $\hat{\alpha}$ at $\hat{\alpha} = 0.5$ (figure 6*c*).

4. The two-line chain: analytical and numerical results

The main objectives of this paper are to determine the critical internal energy level under which the spontaneous separation wave can exist and to find the energy-dependent crack speed. At the

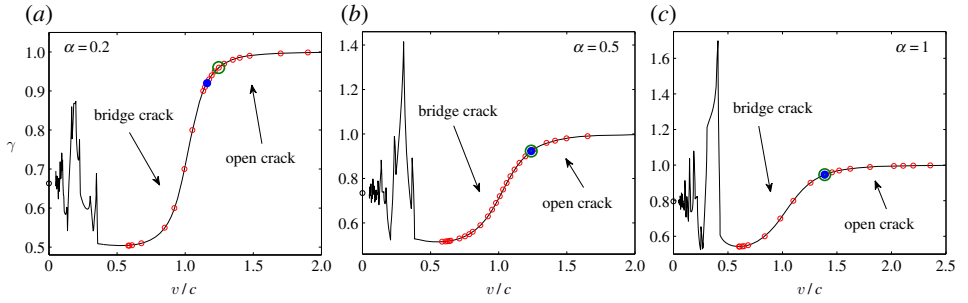

Figure 7. (*a–c*) The spontaneous semi-infinite bridged crack in the two-line chain. The relation between the normalized crack speed, v/c, and the internal energy level, $\gamma = \mathcal{E}/\mathcal{E}_c$ (the solid curves), found analytically based on (2.22) for $\alpha = 0.2, 0.5, 1$. The small open circles situated on the vertical axis correspond to the static state with the semi-infinite bridge crack. The other small open circles on the graphs correspond to the steady-state regimes found by numerical simulations of the corresponding transient problems. The larger solid circle corresponds to the upper bound of the domain of the pure bridged crack. The larger open circle corresponds to the lower bound of the domain of the established partially bridged crack regime, where the length of the bridge zone depends on the level of the internal energy, γ, and the anisotropy parameter, α. These two circles bound the intermediate regime, where the rate of the initially stretched bonds is uniform, whereas the breakage of the initially compressed bonds are chaotic. (Online version in colour.)

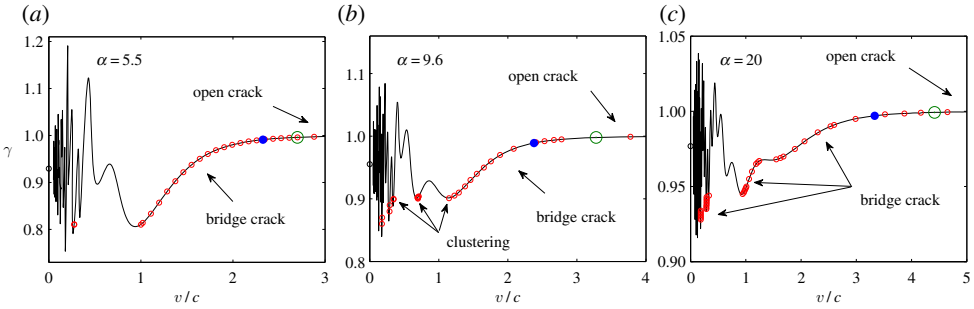

Figure 8. (*a–c*) The $\gamma - v/c$ dependencies as in figure 7 for $\alpha = 5.5, 9.6, 20$. Here, low crack speed regimes with clustering are marked, where there exist crack speed oscillations within the cluster. (Online version in colour.)

same time, in the course of the analysis, we met some unexpected phenomena, such as crack speed oscillations at low internal energy, energy-dependent finite bridge zones at a high energy level, discontinuity in the speed-energy dependence and a notable role of the structure anisotropy. We discuss all this by using the example of the two-line chain.

Note that, in the representation of the numerical results, v is the current speed as before. Recall that for the fully bridged crack it is defined as $2/t_2$, where t_2 is the time between the breakage of two neighbouring initially stretched bonds. The current speed corresponding to the other bond breakage, if it exists, is calculated similarly. In addition, in more complicated cases, the speed averaged over the total time is introduced as $\langle v \rangle = l(t)/t$, where $l(t)$ is the dynamic crack length, the fully/partially bridged crack length or the open crack length, respectively.

The $\gamma - v/c$ relations for some values of α are presented in figures 7–9*a*. In these figures, (*a*) the results where $\gamma > 1$ are not admissible, (*b*) the solid lines are plotted based on the analytical result (2.22), (*c*) the small circles situated on the vertical axis correspond to the static state with the semi-infinite bridge crack. In addition, the results of numerical simulations of the corresponding transient problem are reflected by the circles on the graphs.

Three different regimes were detected. The first is the stable steady-state bridge crack growth as predicted analytically. The upper bound of the corresponding speeds is marked by a larger

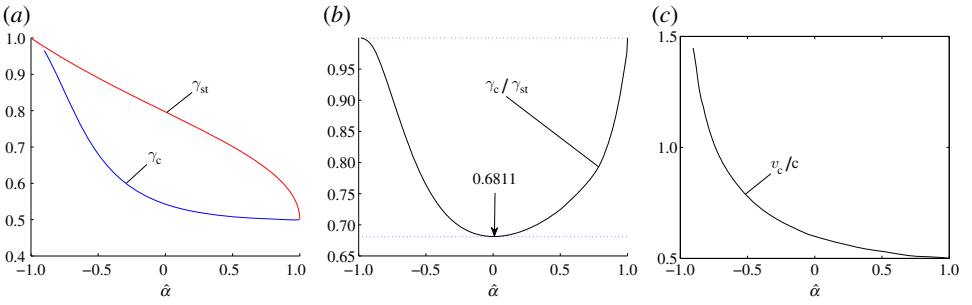

Figure 9. The spontaneous semi-infinite bridged crack in the two-line chain. The comparative plots of the critical values of $\gamma_c(\hat{\alpha})$ (the minimal values of γ under which the steady-state regime of the spontaneous crack growth exists), the corresponding quasi-static dependence, γ_{st} (*a*,*b*), and the crack speed, $v(\hat{\alpha})/c$, corresponding to $\gamma = \gamma_c$. (*c*) Recall that γ_c corresponds to the minimum γ on the smooth parts of the plots in figure 7. The manifestation of the dynamic amplification factor (see [13]), which leads to the considerable decrease of the minimal γ in dynamics, can be clearly seen. (Online version in colour.)

bold circle. Next, there is a higher speed region, where the crack growth is accompanied by an irregular breakage of the initially compressed bonds; it is bounded by the larger open circle. Finally, at the right of the latter there exists the high-speed region, corresponding to the stable steady-state crack growth. In this region, however, only a finite bridge zone remains adjacent to the crack front, whereas the fully open crack front propagates with the same speed at a distance. Thus, the spontaneous crack growth regime changes as the internal energy approaches the critical value (that results in unlimited crack speed growth); however, the analytically and numerically obtained crack speeds remain equal for any energy level, for any crack speed. Below, we discuss the findings of numerical simulations in more detail.

The lower bound of γ-region, $\gamma_c < \gamma < 1$, where the spontaneous crack can propagate, as a function of the anisotropy parameter, $\hat{\alpha}$, versus the corresponding crack-initiation dependence, γ_{st}, obtained in [1], is presented in figure 9*a*,*b*. The crack-speed dependence corresponding to $\gamma = \gamma_c$ is shown in figure 9*c*.

5. The numerical simulations

(a) The basic aspects

The numerical simulations were conducted with the aim of determining the domains of validity of the analytical solutions, and to reveal possible phenomena which could not be observed in the framework of the above analytical studies. Two different cases were investigated numerically.

— Case 'A' corresponds to an 'infinite' chain, the ends of which are far enough from the crack not to reveal themselves in the crack region during the calculations. Initially, the structure is separated into two parts, the intact chain (at the right) and the chain without even bonds (at the left). The spontaneous crack propagation is initiated by removing the first even bond. This structure is assumed to reflect the steady-state regime, or at least to approach it with a good accuracy in a reasonable time.
— Case 'B' represents a 'semi-infinite' waveguide, where the left part is absent. We use this structure to see what happens if the fracture starts from the left end of the waveguide or inside the 'infinite' structure propagating in both directions. In this case, the wave emitted by the crack completely reflects and, under some conditions, the reflected wave can propagate faster than the crack and can influence its speed.

Note that the emitted wave with the left-directed group velocity has the phase speed equal to the crack speed. At the same time, the reflected wave directed to the right differs by the

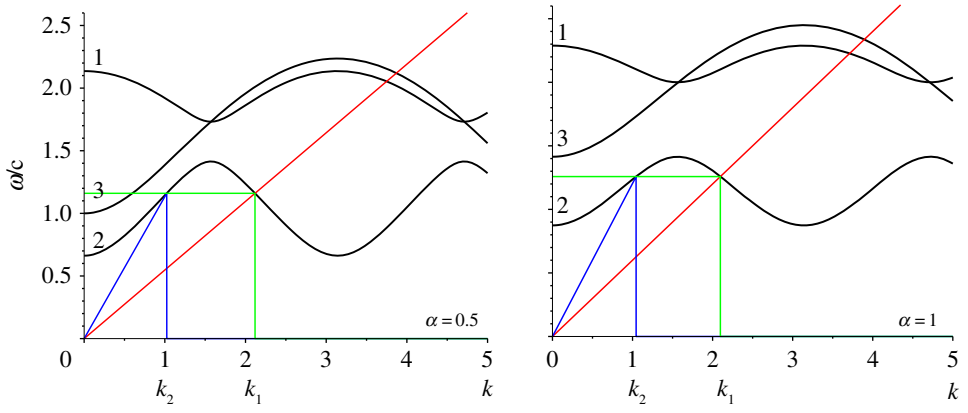

Figure 10. Dispersion curves for the chain without even bonds (1,2) and for the intact chain (3). The wavenumbers of the emitted wave (k_1) and the reflected wave (k_2) under the crack speed $v = 0.54775c$ for $\alpha = 0.5$ and $v = 0.6c$ for $\alpha = 1$. Wave frequency $\omega = vk_1$. (Online version in colour.)

wavenumber and, therefore, interacts with the propagating crack with a non-zero frequency. Thus, it could perturb the steady crack growth.

In spite of the presence of the left part of the chain, some reflection also occurs in the case 'A'. This is because the left part is not initially synchronized with the steady-state motion. Clearly, this is not a total reflection. Thus, cases 'A' and 'B' are different, which allows us to trace the role of the left-hand end condition in more detail.

As can be seen below, a wider spectrum of fracture modes corresponds to case 'B', whereas the stable steady-state modes appear identical for both cases. With this in mind, we mainly consider case 'B', and it assumed everywhere, unless case 'A' is noted. The latter differs mainly by the absence of some subcritical disordered regimes. Note that such regimes are not observed in the case of large values of α.

To elucidate the peculiarities of the wave reflection, consider dispersion relations for the case 'A'

$$\left.\begin{aligned} &\omega_{1,2} = c\sqrt{2+\alpha \pm \sqrt{\alpha^2 + 4\cos^2 k}} \quad \text{(for the left part)} \\ \text{and} \quad &\omega_3 = c\sqrt{2\alpha + 4\sin^2\left(\frac{k}{2}\right)} \quad \text{(for the right part).} \end{aligned}\right\} \tag{5.1}$$

The dispersion curves for $\alpha = 0.5$ and $\alpha = 1$ are presented in figure 10. First, we note that, to reach the crack front, the reflected wave group velocity must be greater than the crack speed

$$v_g = \frac{d\omega_2}{dk} > v = \frac{\omega}{\pi - k}. \tag{5.2}$$

Based on the dependence of the crack speed under minimal internal energy, figure 9*c*, we found that this inequality is not valid for any $\alpha > 1.2$. Thus, the conditions at the left end could matter only in the case $\alpha < 1.2$.

An explicit finite-difference algorithm is used for the calculation of a respective system of ordinary differential equations governing the motion of chain masses. The required accuracy is achieved and verified. Both even (initially stretched) and odd (initially compressed) bonds are subjected to the limiting elongation condition. Simulations of the transient problem have been conducted for several values of the anisotropy parameter α, whose role appeared crucial in some respects. The lattice spacing and the long wave speed are taken as the length and speed units.

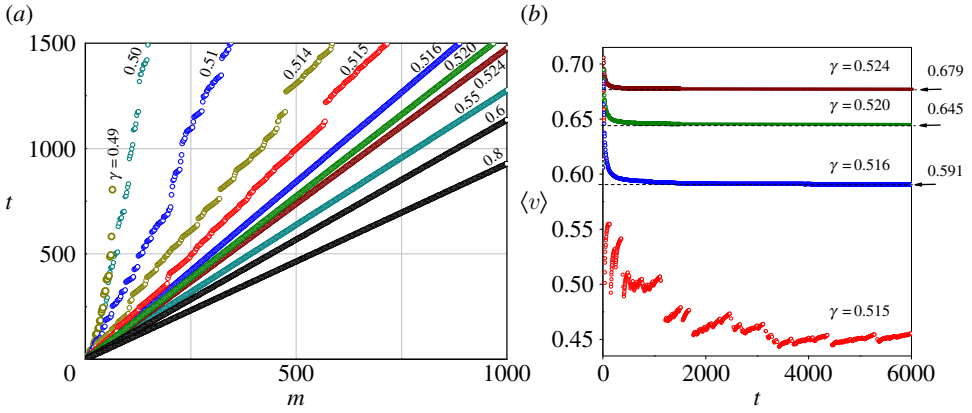

Figure 11. Results of the numerical simulations. The spontaneous bridge crack for $\alpha = 0.5$. The plots for the current length of the pure bridged crack, $m(t)$ (*a*), and some of the corresponding average speeds (*b*). The lack-of-energy transient regimes for $0.500 \leq \gamma \leq 0.515$ and the establishing steady-state modes for $\gamma \geq 0.516$. (Online version in colour.)

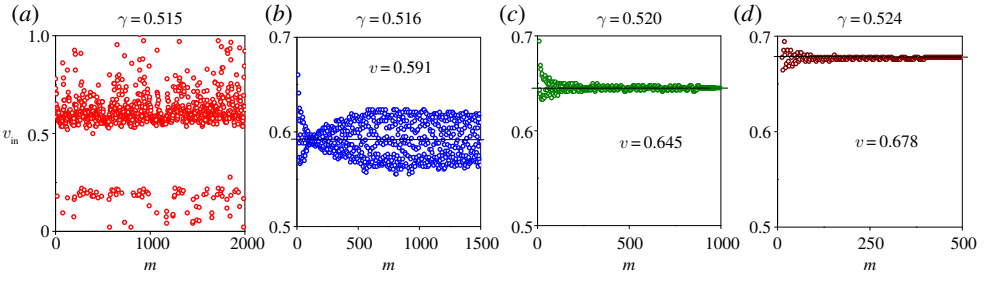

Figure 12. (*a–d*) Results of the numerical simulations. The spontaneous bridge crack for $\alpha = 0.5$. The current speed distributions. It is seen how the speed stabilizes as internal energy increases, and in time tends towards the steady-state mode. (Online version in colour.)

(b) Anisotropic chain corresponding to $\alpha = 0.5$

The plots for the current length of the fully bridged crack as a function of time, $m(t)$-plots, and some of the corresponding average speeds are presented in figure 11 for a number of internal energy levels. The steady-state regime exists for any value of $\gamma \geq 0.516$, whereas the breakage in the range $0.49 \leq \gamma \leq 0.515$ continues but is not established. Note that the analytical minimum is 0.5150 (figure 7*b*). The plots show that the steady-state regime is established more rapidly as the internal energy increases. The current speed distributions are shown in figure 12. The high-amplitude crack speed oscillations about the averaged speed are seen to exist at the minimal energy level, and quickly vanishes as the energy increases. Distribution of the instantaneous speeds has similar profiles for all values of $\gamma < 0.5150$ and is not presented here.

The comparative results for the case 'A' are presented in figure 13. It can be seen that the stable regimes are the same. The only difference concerns the low-speed-disordered regimes corresponding to $\gamma < 0.5160$. Comparing figures 11 and 13, we conclude that the range of the subcritical energy modes essentially decreased for the case 'A' (the open waveguide), as we have expected above. The special case, $\gamma = 0.5150$, which coincides with the analytically predicted lower bound of the energy, remains the same in both cases. Some new subcritical modes appear between the stable regime $\gamma = 0.5160$ and the lower bound regime. The instability of the steady-state mode at the minimal bound of the energy occurs owing to a weak certainty of

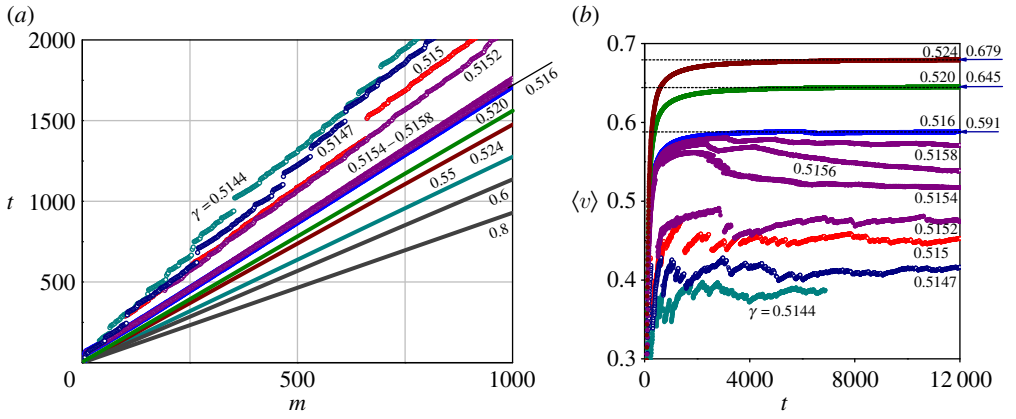

Figure 13. Case 'A': results of the numerical simulations. The spontaneous bridge crack for $\alpha = 0.5$. The plots for the current length of the pure bridged crack, $m(t)$, (*a*) and some of the corresponding average speeds (*b*). The established steady-state modes appear for $\gamma \geq 0.516$ and completely coincide with case 'B' (figure 11). (Online version in colour.)

the minimum. For larger values of α where the minimum is more pronounced, the lower bound mode is stable.

In connection with the discussed topic, we note that the internal energy stored in the chain is at least twice as much as the bound strain energy. When the crack propagates, the energy excess outflows from the crack front with the emitted wave. If the wave meets an obstacle (such as in case 'B'), then the reflective wave arise which may provide additional energy to the fracture. However, in the subcritical regimes, this energy is still not sufficient for the steady-state mode to exist. As the result, the disordered crack spreading occurs in a range at $\gamma < 0.5160$ as discussed above. This is why this range is much smaller for the open waveguide in comparison with that in case 'B'.

Note that the profiles of the instantaneous speeds in the energy range $0.5150 < \gamma < 0.5160$ are still the same as shown in figure 12*a*; however, the lower cloud becomes less dense with increasing γ and disappears at $\gamma = 0.5160$, where a 'fish-like' structure occurs (compare with figure 12*b*). As γ increases further, the dispersion in the speed distribution decreases to zero.

(c) Isotropic chain ($\alpha = 1$)

The plots of the crack tip position as a function of time and some of the corresponding average speeds are presented in figures 14 and 15 (compare with figures 11 and 12 related to $\alpha = 0.5$). The extremely sharp interface can be observed between the steady-state and transient regimes at the energy minimum. It is seen how dramatically the speeds, both the averaged and current speeds, change under a barely notable increase in the energy level from $\gamma = 0.542630$ to 0.542631. With this tiny step, the crack propagation mode is transformed from almost chaotic to steady-state. Note that the analytical minimum (figure 7*c*) is 0.5426. Again, when the open waveguide (case 'A') is considered, the subcritical energy range becomes far more narrow, whereas for the values $\gamma > 0.5426$, no difference with that in the case 'B' is observed.

As the energy approaches the upper critical value, the compressed bonds begin to break at an energy-dependent distance behind the crack front. This is shown in figure 16. In the numerically examined transient problem, the odd-bond breakage begins at a distance from the starting point of the dynamic crack. The latter distance as well as the former vanishes as the energy approaches the upper critical bound.

In a general case of the steady-state regime, the length of the bridge crack zone is energy-independent, and its rear bound propagates with the same constant speed as the crack front. As can be seen in figure 16*c*, there is a forward–backward splitting, the bonds break in the order $2m \to 2m-3 \to 2m+2 \to 2m-1 \to \ldots$.

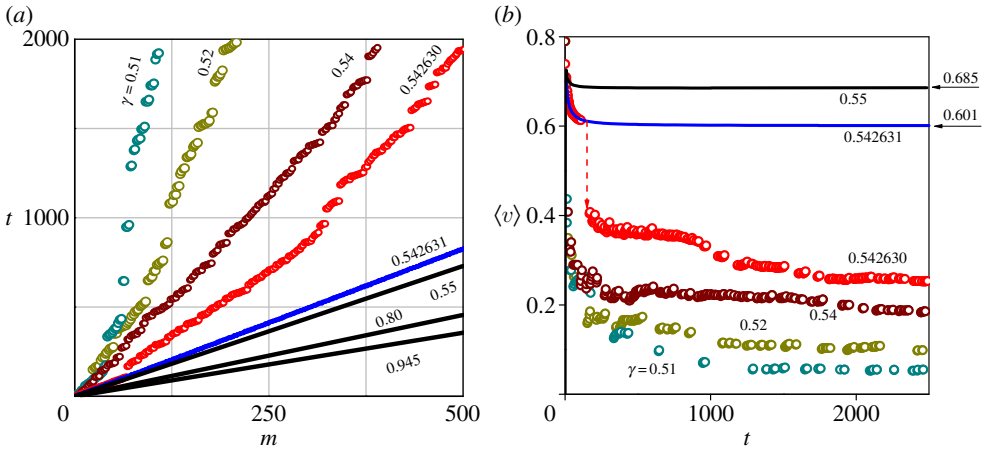

Figure 14. Results of the numerical simulations. The spontaneous bridge crack for $\alpha = 1$. The plots for the current length of the fully bridged crack, $m(t)$ (*a*), and some of the corresponding average speeds (*b*). The extremely sharp interface can be observed between the steady-state and transient regimes at the energy minimum. It is seen how dramatically the speeds, both the averaged and current speeds, change under a barely notable increase in the energy level from $\gamma = 0.542630$ to 0.542631. With this tiny step, the crack propagation mode is transformed from almost chaotic to steady-state. (Online version in colour.)

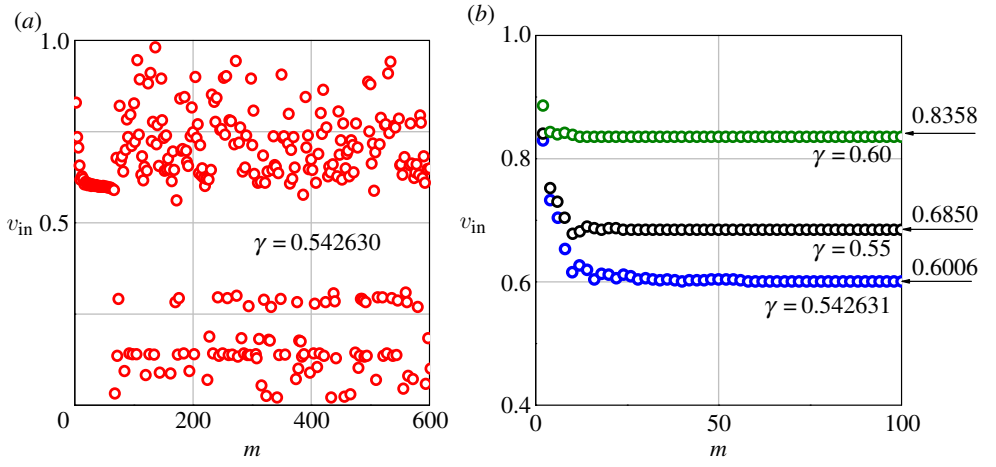

Figure 15. (*a*,*b*) Results of the numerical simulations. The spontaneous bridge crack for $\alpha = 1$. The current speed distributions for some values of γ. The dramatic change is seen with a tiny change in the internal energy, from $\gamma = 0.542630$ to 0.542631. (Online version in colour.)

In figure 17*a*,*b*, the profiles of the fracture are shown for two different values of the internal energy, $\gamma = 0.6$ and $\gamma = 0.948$ which correspond to the bridge crack and the open crack regimes, respectively.

(d) Anisotropic chain corresponding to $\alpha = 9.6$

Such a stiff-transverse-bond structure presents us with some notable effects: (i) there exist here stable steady-state regimes corresponding to the oscillating part of the $\gamma - v/c$ diagram below the smooth minimum of the internal energy (compare figures 18 and 8*b*). (ii) In some of the energy ranges, the speed is energy-independent (see two upper lines in figure 18*a*). This is because the regime corresponds to very narrow kinks in the $\gamma - v/c$ diagram as can be seen in

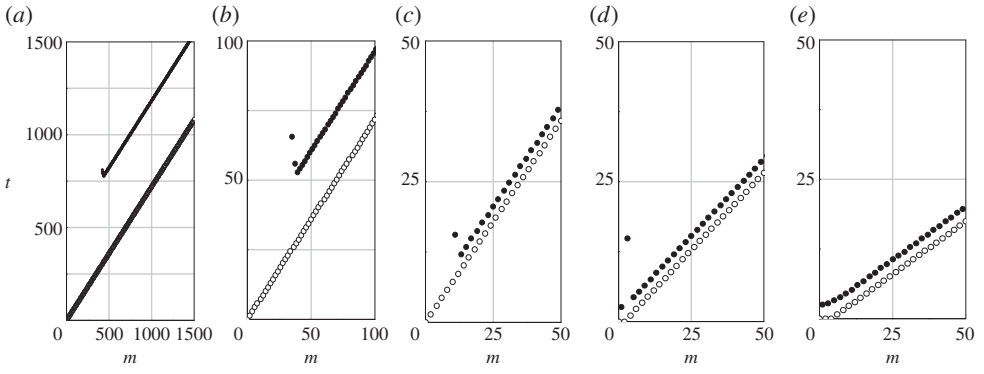

Figure 16. Results of the numerical simulations. The propagation of a partially bridged crack. The modes are presented where the initially compressed bonds break at an energy-dependent distance behind the crack front. In the numerically examined transient problem, the odd-bond breakage begins at a distance from the starting point of the dynamic crack. The latter distance as well as the former vanishes as the energy approaches the upper critical bound. In a general case of the steady-state regime, the length of the bridge crack zone is invariable. As can be seen in plot (*c*), there is a forward–backward splitting, the bonds break in the order $2m \to 2m-3 \to 2m+2 \to 2m-1 \to \ldots$. (*a*) $\gamma = 0.946$ (*b*) $\gamma = 0.947$ (*c*) $\gamma = 0.948$ (*d*) $\gamma = 0.990$ (*e*) $\gamma = 0.999$.

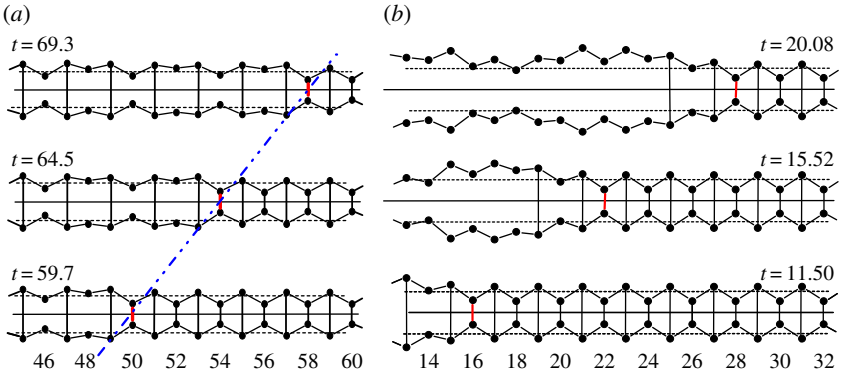

Figure 17. Profiles of the chain at the moments immediately before the breakage of the selected links. Panels (*a*,*b*) correspond to the energy levels $\gamma = 0.6$ and $\gamma = 0.948$, respectively. Links $m = 50$, 54 and 58 are destroyed at times $t = 59.7$, 64.5 and 69.3, respectively, when $\gamma = 0.6$, whereas for the energy level $\gamma = 0.948$, the numbers are $m = 16$, 22 and 28 for $t = 11.5$, 15.52 and 20.08. Note that in the latter case, bonds $m \leq 11$ remains intact for the whole process. Horizontal lines show the position of the masses along the bridged crack part of the structure at the static condition. The blue dashed line at the left corresponds to the steady-state crack movement with the constant speed, $v = 0.836$. In figure 17*b*, the crack moves with the supersonic speed, $v = 1.399$. (Online version in colour.)

figure 8*b*. (iii) The three-even-bond clustering arises at $\gamma = 0.900$. The current speeds in the cluster correspond to the minima shown in figure 8*b* for the latter level of the energy. The average and current speeds corresponding to the plots in figure 18*a* are shown in figure 18*b*,*c*, respectively.

(e) Main results of the numerical simulations

We now list the main findings of the numerical simulations.

— The relations between the crack speed and the internal energy, $\gamma - v/c$ diagrams, obtained analytically for the steady-state regimes and numerically for established crack propagation in the corresponding transient problems, fully coincide.

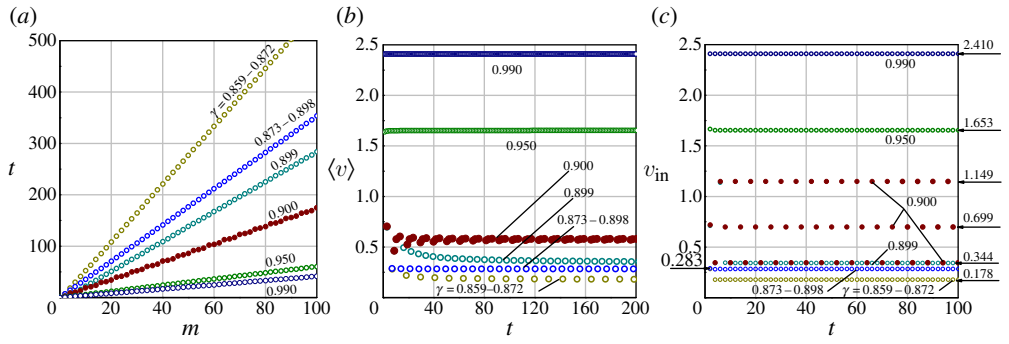

Figure 18. Results of the numerical simulations. The spontaneous bridge crack for $\alpha = 9.6$. The plots for the current length of the fully bridged crack, $m(t)$ (*a*), and some of the corresponding average (*b*) and current (*c*) speeds. The three-even-bond clustering can be observed at $\gamma = 0.900$. The current speeds in the cluster correspond to the minima shown in figure 8*b* for the latter level of the energy. (Online version in colour.)

— The transition from disordered regimes to the established ones occurs on a very narrow interval. Stable steady-state regimes start from a value of γ exceeding the analytically obtained minimum by 1/500 ($\alpha = 0.5$) and 1/500 000 ($\alpha = 1$).
— In special cases, where the crack speed appears to be non-uniquely defined, as shown in figure 8, it may oscillate between the separate minima found analytically. In the case of such clustering, the instantaneous crack speeds observed within the cluster coincide with the corresponding values predicted analytically.
— For large values of the anisotropy parameter α, the $\gamma - v/c$ diagram oscillates intensively at low crack speeds. As the result, the global minimum of γ appears below that defined for the smooth part of the diagram. The numerical simulations show that, in such cases, there exist stable propagation regimes corresponding to the sharp global minimum.
— The spontaneous crack can spread under a subcritical energy level, when it is somewhat below the analytically found minimum. The width of the corresponding subcritical γ-region depends on the condition at the left. Remaining narrow, it reaches its maximum in the case with the total reflection.
— The regions of the internal energy corresponding to different crack speed regimes depend essentially on anisotropy parameter α.
— At high levels of the internal energy, the pure bridged crack mode changes to the partially bridged one, where only a finite bridge zone remains adjusted to the crack front (figure 19). The length of the bridge–crack zone decreases to zero as γ increases. There also exists an intermediate region, where the bridged crack growth is accompanied by irregular breakage of the initially compressed bonds. The breakage of the compressed bonds, however, does not influence the crack speed, because it is supersonic in these cases. Although no energy flux is required, to overcome the energy barrier in the bond breakage, a transfer of energy from one bond to another is needed. In the supersonic regime, such a transfer is possible because the between-the-bond links are massless. Nevertheless, any event, taking place at a distance several spans behind the supersonic crack front, cannot affect the crack speed. So, when the odd bonds break at a distance, the even-bond breakage must propagate as predicted by the steady-state analytical solution obtained for the bridged crack, and this is confirmed by the numerical simulations.

Note that the possibility of supersonic crack propagation in massless-bond discrete lattices was first shown analytically in [17]. Then, in the application to fracture and phase transition, this phenomenon is discussed in more detail in [8, sections 11–13], where the steady-state formulation is used. Analytical considerations and results of multiple numerical simulations of the respective transient regimes are presented in [19] for the square and triangular lattices, and in [20] for some

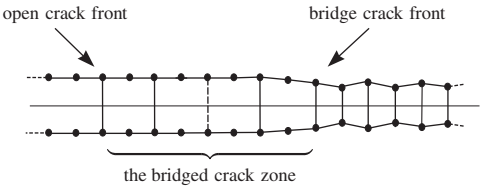

Figure 19. The chain structure in the steady-state open crack regime, where two fronts, the bridged crack front and the open crack front behind it, move with the same speed.

triangular lattice strips. In these publications, in contrast to the present paper, the energy on the crack path appeared owing to lattice oscillations or a static prestress by an external load applied over the body.

6. Conclusion

The problem of spontaneous crack propagation under the internal energy is formulated and solved. Analytical solutions are obtained for a general periodic structure, where only the crack–path interface is specified. The results for the general structure are presented in terms of a non-specified dynamic Green's function. The results for an anisotropic lattice and a chain are presented explicitly and discussed in detail. The analytical solutions are derived using the selective discrete transform introduced in [1].

The lower bound of the internal energy and the crack-speed–energy relations are determined. For the lattice and chain, the results are presented as functions of an anisotropy parameter. The solutions evidence that the crack can propagate at subsonic as well as supersonic speeds. The latter grows unboundedly as the energy level approaches the upper limit.

In some cases, the steady-state analytical solutions suggest crack-speed instabilities. This can occur when the solution does not define the crack speed uniquely. The numerical simulations confirm that crack speed oscillations really occur under such conditions.

Numerical simulations of the corresponding transient problem for the chain demonstrate the stability and validity of the steady-state analytical solutions. In addition, in the numerical simulations, other regimes are observed, such as (i) a disordered slow crack spreading in a very narrow subcritical range of the internal energy, (ii) clustering with crack speed oscillations, also at the lower boundary of the energy and (iii) breakage of the initially compressed bonds under a high level of the energy. The latter phenomenon does not affect the crack speed because, in this case, it is supersonic. The transition from the disordered regimes to the established ones occurs on a very narrow interval. Stable steady-state regimes start from a value of γ exceeding the analytically obtained minimum by 1/500 ($\alpha = 0.5$) and 1/500 000 ($\alpha = 1$).

Finally, we note that along with the spontaneous crack propagation, the crack dynamics under the combined action of external forces and the internal energy is of interest. We consider the latter problem separately.

Acknowledgements. G.M. and L.S. acknowledge support from the FP7 Marie Curie grant no. 284544-PARM2. We also appreciate valuable comments from the reviewers.

References

1. Mishuris GS, Slepyan LI. 2014 Brittle fracture in a periodic structure with internal potential energy. *Proc. R. Soc. A* **470**, 20130821. (doi:10.1098/rspa.2013.0821)
2. Marder M, Gross S. 1995 Origin of crack tip instabilities. *J. Mech. Phys. Solids* **43**, 1–48. (doi:10.1016/0022-5096(94)00060-I)
3. Holland D, Marder M. 1999 Cracks and atoms. *Adv. Mater.* **11**, 793–806. (doi:10.1002/(SICI)1521-4095(199907)11:10<793::AID-ADMA793>3.0.CO;2-B)

4. Mishuris GS, Movchan AB, Slepyan LI. 2008 Dynamics of a bridged crack in a discrete lattice. *Q. J. Mech. Appl. Math.* **61**, 151–160. (doi:10.1093/qjmam/hbm030)
5. Mishuris GS, Movchan AB, Slepyan LI. 2009 Localised knife waves in a structured interface. *J. Mech. Phys. Solids* **57**, 1958–1979. (doi:10.1016/j.jmps.2009.08.004)
6. Slepyan LI, Ayzenberg-Stepanenko MV. 2002 Some surprising phenomena in weak-bond fracture of a triangular lattice. *J. Mech. Phys. Solids* **50**, 1591–1625. (doi:10.1016/S0022-5096(01)00141-7)
7. Slepyan LI, Troyankina LV. 1984 Fracture wave in a chain structure. *J. Appl. Mech. Techn. Phys.* **25**, 921–927. (doi:10.1007/BF00911671)
8. Slepyan LI. 2002. *Models and phenomena in fracture mechanics*. Berlin, Germany: Springer.
9. Slepyan L, Cherkaev A, Cherkaev E. 2005 Transition waves in bistable structures. II. Analytical solution: wave speed and energy dissipation. *J. Mech. Phys. Solids* **53**, 407–436. (doi:10.1016/j.jmps.2004.08.001)
10. Vainchtein A. 2010 The role of spinodal region in the kinetics of lattice phase transitions. *J. Mech. Phys. Solids* **58**, 227–240. (doi:10.1016/j.jmps.2009.10.004)
11. Munawar Chaudhri M. 2009 The role of residual stress in a Prince Rupert's drop of soda-lime glass undergoing a self-sustained and stable destruction/fracture wave. *Phys. Status Solidi A* **206**, 1410–1413. (doi:10.1002/pssa.200925006)
12. Silverman MP, Strange W, Bower J, Ikejimba L. 2012 Fragmentation of explosively metastable glass. *Phys. Scr.* **85**, 065403 (9 pp). (doi:10.1088/0031-8949/85/06/065403)
13. Slepyan LI. 2000 Dynamic factor in impact, phase transition and fracture. *J. Mech. Phys. Solids* **48**, 927–960. (doi:10.1016/S0022-5096(99)00061-7)
14. Mishuris GS, Movchan AB, Slepyan LI. 2007 Waves and fracture in an inhomogeneous lattice structure. *Waves Random Complex Media* **17**, 409–428. (doi:10.1080/17455030701459910)
15. Mishuris GS, Movchan AB, Bigoni D. 2012 Dynamics of a fault steadily propagating within a structural interface. *SIAM J. Multiscale Modell. Simul.* **10**, 936–953. (doi:10.1137/110845732)
16. Slepyan LI. 1981 Dynamics of a crack in a lattice. *Sov. Phys. Dokl.* **26**, 538–540.
17. Slepyan LI. 1981 Crack propagation in high-frequency lattice vibration. *Sov. Phys. Dokl.* **26**, 900–902.
18. Slepyan LI, Mishuris GS, Movchan AB. 2010 Crack in a lattice waveguide. *Int. J. Fract.* **162**, 91–106. (doi:10.1007/s10704-009-9389-5)
19. Guozden TM, Jagla EA, Marder M. 2010 Supersonic cracks in lattice models. *Int. J. Fract.* **162**, 107–125. (doi:10.107/s10704-009-9426-5)
20. Jia YJ, Zhu WP, Li T, Liu B. 2012 Study on the mechanisms and quantitative law of mode I supersonic crack propagation. *J. Mech. Phys. Solids* **60**, 1447–1461. (doi:10.1016/j.jmps.2012.04.008)